

A. Nicholas Hayes¹

University of Oxford, Department of Mathematics

Andrew Wiles Building, Woodstock Rd, Oxford OX2 6GG, United Kingdom

(Dated: December 2, 2025)

Extending a framework originally proposed by Cencetti et al.¹, we investigate a topological control mechanism for mediating Turing patterns on unweighted, undirected networks. Our primary contribution is proving boundedness results involved in targeted destabilization, in which we map Laplacian mode shifts to structural interventions. Through numerical simulations, we show the efficacy of this control scheme on a range of graph models, establishing theoretical expectations for the special case of the ring lattice. This work stands against a backdrop of real-world applications, moving the needle towards better understanding and engineering of network-driven pattern formation.

Though originally studied in continuous media, Turing patterns on network structures offer a unique opportunity to model discrete real-world systems. Existing literature has shown that pattern emergence can be induced by tuning system parameters; however, in practice, it may be difficult to alter the dynamics of real systems. Rather than manipulating the system, we can instead manipulate the topology of the network on which the system operates, wherein structural changes may more readily correspond to real-world scenarios. It is thus a worthy endeavor to explore control mechanisms for Turing pattern formation on networks, wherein we strategically rewire networks to induce/suppress patterns. With applications in epidemiology, ecological modeling, cell networks, and more, this work aims to shed insight on real-world network phenomena by analyzing the results of a targeted re-wiring procedure.

I. INTRODUCTION

Turing patterns², first introduced by Alan Turing in 1952, describe the spontaneous emergence of spatial heterogeneity in reaction-diffusion systems. Originally formulated for continuous media, the theory has since been extended to discrete domain. The network-based formulation has proven quite successful in myriad domains, including but not limited to neuroscience^{3–6}, developmental biology^{7,8}, ecology^{9–12}, and epidemiology^{13–16}. In such domains, tuning system parameters or reaction kinetics may be infeasible; modifying network structures may offer a practical and interpretable alternative form of control.

In this work, we develop and analyze a novel topological control scheme that targets specific Laplacian modes for destabilization, inducing Turing patterns. Building on existing spectral-shift frameworks, we introduce a binarization step that enables recovery of an unweighted graph after shifting a target Laplacian mode. Through analytical and numerical results, we characterize when and how such interventions succeed, with particular attention to the ring lattice, where closed-form bounds can be established. Our findings advance the theoretical toolkit for engineering patterns in networked systems and suggest new directions for structural interventions in

complex dynamical systems.

A. A Network Reaction-Diffusion System

We start with a general vectorized form of the network reaction-diffusion system.

$$\frac{d}{dt} \mathbf{w}_i = \underbrace{\mathcal{F}(\mathbf{w}_i)}_{\text{reaction term}} + K \sum_{j=1}^N A_{ij} \underbrace{\mathcal{G}(\mathbf{w}_j - \mathbf{w}_i)}_{\text{diffusion term}}$$

where $\mathbf{w}_i \in \mathbb{R}^m$, $\mathcal{F} : \mathbb{R}^m \rightarrow \mathbb{R}^m$, $\mathcal{G} : \mathbb{R}^m \rightarrow \mathbb{R}^m$, and $K \in \mathbb{R}$ is constant. The dynamics of m species of interest are locally specified at node i by \mathcal{F} (the *reaction*), whereas \mathcal{G} controls the dynamics of species moving between nodes i and j for $j \in \mathcal{N}_i$ (the *diffusion*). Following inspiration from activator-inhibitor systems, we assume $m = 2$ and a linear, species-independent¹⁷ design of \mathcal{G} , allowing us to decompose the general formulation into the commonly studied two-species system. Namely, when

$$\mathbf{w}_i = \begin{pmatrix} u_i \\ v_i \end{pmatrix}, \quad \mathcal{F}(\mathbf{w}_i) = \begin{pmatrix} f(u_i, v_i) \\ g(u_i, v_i) \end{pmatrix}, \quad \mathcal{G} = \begin{pmatrix} c_u(u_j - u_i) \\ c_v(v_j - v_i) \end{pmatrix} \Rightarrow$$

$$\begin{cases} \frac{d}{dt} u_i = f(u_i, v_i) + D_u \sum_{j=1}^N L_{ij} u_j \\ \frac{d}{dt} v_i = g(u_i, v_i) + D_v \sum_{j=1}^N L_{ij} v_j \end{cases} \quad (1)$$

where $D_u = Kc_u$ and $D_v = Kc_v$ represent diffusion coefficients. It is worth clarifying that we define the Laplacian as $L = A - D$, following the conventions of existing literature on network reaction-diffusion systems. For the remainder of this work, we assume connected graphs unless explicitly stated otherwise.

Though existing work has dealt with the linear, two-species case¹⁸ through the use of multigraphs, wherein each species diffuses across its own distinct edge-set connecting a shared set of nodes, this work allows all species to diffuse across a shared edge-set.

B. Pattern-Enabled Systems

In the absence of diffusion, we assume there exists a homogeneous, linearly stable stationary state, (u_i^*, v_i^*) . We note that stationary Turing instabilities on networks are frequently subcritical bifurcations and can exhibit substantial multistability. Hence, controlling which eigenmode destabilizes should not be interpreted as direct control over the final nonlinear pattern. Linearizing perturbations about the stationary state gives rise to the following dispersion relation that connects $\lambda_\alpha, \Lambda_\alpha$, and system parameters:

$$\lambda_\alpha \begin{pmatrix} 1 \\ b_\alpha \end{pmatrix} = \begin{pmatrix} f_u + D_u \Lambda_\alpha & f_v \\ g_u & g_v + D_v \Lambda_\alpha \end{pmatrix} \begin{pmatrix} 1 \\ b_\alpha \end{pmatrix} \quad (2)$$

We henceforth distinguish between λ_α and Λ_α as the dispersion and Laplacian eigenvalues respectively. As a matter of notation, f_u, f_v, g_u , and g_v represent partial derivatives of the reaction terms with respect to each species. The full derivation for the dispersion relation can be found in the supplementary materials of Cencetti et al.'s 2018 work on pattern invariance¹⁹, with additional a number of works^{13,20} providing additional context. From the dispersion relation, we note

$$\det(J_\alpha) = \Lambda_\alpha^2 D_u D_v + \Lambda_\alpha (f_u D_v + g_v D_u) + f_u g_v - f_v g_u$$

For the system to be unstable, we must have $\det(J_\alpha) < 0$, corresponding to $\text{Re}(\lambda_\alpha) > 0$. It is apparent that by strategically manipulating diffusion coefficients²¹ and/or the reaction functions f and g , we can induce instability; however, when holding such system parameters constant, the dispersion relation becomes a function of Laplacian eigenvalues. As the Laplacian spectrum serves as a proxy for the structure of the underlying network, we can thus map instability arising from Laplacian eigenvalues to recovered network structures.

We introduce the descriptor *pattern-enabled* to describe systems whose parameters, when held constant, allow for the formation of patterns. Importantly, this does not guarantee the presence of Turing patterns, as we still depend on the Laplacian eigenvalues of the network.

C. Structural Tuning

We now transition to pattern control by reviewing a "global topological control" mechanism¹, in which Cencetti et al. outline a procedure to manually push Laplacian eigenvalues into the stability region. The procedure is as follows:

1. For each mode l , choose a δ_l such that $(\Lambda_l + \delta_l)$ yields a dispersion relation eigenvalue with negative real component.²² If already stable, set $\delta_l = 0$.
2. Define a diagonal matrix D^* such that $D_{ll}^* = \delta_l$.
3. Calculate $L^* = \Phi D^* \Phi^T$ where Φ is a unitary matrix with orthonormal eigenvectors of L as its columns.²³
4. Set $L_c = L + L^*$, henceforth deemed the *controlled Laplacian*

As L_c is Laplacian¹, we can interpret it as representing an underlying graph. Though the shift from $L \rightarrow L_c$ is, superficially, a strategy to shift eigenvalues, the underlying graphs generated by L and L_c uncover the structural changes needed to mediate stabilization. Ultimately, we have created a Laplacian matrix whose eigenvalues are all stable by construction.

We now take a closer look at this transformation, paying particular attention to network structure. For the following observations, let \mathbf{G} and \mathbf{G}_c denote the graphs of interest recovered from L and L_c respectively. We additionally order δ -shifts such that $\delta_1, \delta_2, \dots, \delta_N$ correspond to the ranked eigenvalues, $\Lambda_1 < \Lambda_2 < \dots < \Lambda_N = 0$

For undirected \mathbf{G} , (i.e. L, L_c are both symmetric), the transformation $L \rightarrow L_c$ is equivalent to re-weighting each possible edge of \mathbf{G} .

We can write the re-weighting exactly by taking a closer look at off-diagonal entries of L_c .

$$\begin{aligned} (L_c)_{ij} &= \sum_{k=1}^n (\phi^{(k)})_i (\phi^{(k)})_j (\Lambda_k + \delta_k) \\ &= \sum_{k=1}^n (\phi^{(k)})_i (\phi^{(k)})_j (\Lambda_k) + \sum_{k=1}^n (\phi^{(k)})_i (\phi^{(k)})_j (\delta_k) \\ &= L_{ij} + \underbrace{\sum_{k=1}^n (\phi^{(k)})_i (\phi^{(k)})_j (\delta_k)}_{:=\eta(i,j)} \end{aligned}$$

Here we see the transformation as an additive re-weighting by $\eta(i,j)$. With no further assumptions on \mathbf{G} , we make no further claims on the sign or bounds of $\eta(i,j)$. Thus, L_c represents a weighted, undirected graph that allows for negative weights²⁴. As a final note, this re-weighting operates on edges ($L_{ij} \neq 0$) and non-edges ($L_{ij} = 0$) alike.

D. Localization

It is a well known phenomenon that eigenvectors tend to localize under certain conditions^{25,26}, often measured using an inverse participation ratio (IPR)²⁷.

$$\text{IPR}(\phi) = \frac{\sum_i (\phi_i)^4}{(\sum_i (\phi_i)^2)^2} \quad (3)$$

Bounded between $\frac{1}{N}$ and 1, the IPR indicates the degree to which an eigenvector's "weight" is spread across its components; highly localized eigenvectors, where just a few components are responsible for the majority of the vector's weight, will have higher IPRs. It has been empirically shown that localization effects are generally more pronounced as degree heterogeneity increases. An in-depth treatment of Laplacian eigenvector localization for large random networks is given by Hata and Nakao²⁵.

$\eta(i,j)$ is strongly influenced by localization. If any $\phi^{(l)}$ is highly localized around some subset of nodes, then δ_l 's contribution to $\eta(i,j)$ will be heavily weighted if i, j are included in the subset and hardly weighted otherwise. Accordingly, if all eigenvectors are highly localized, then $\eta(i,j)$ is essentially

controlled by only the eigenvectors wherein i, j are in the localization subset. This observation is crucial in building intuitions for later numerical simulations on graph models that exhibit strong localization.

II. TARGETED DESTABILIZATION

The topological control mechanism above, when implemented, prevents pattern formation on an undirected graph by re-weighting its edges, with no sign-restriction on weights. In our work, we instead ask whether we can develop a control mechanism where, rather than re-weighting, we add/delete/re-wire unweighted edges to induce instability on targeted modes. The main distinction between the prior procedure¹ and ours is that we do not allow edges to retain weights; they are either present or not.

Suppose we have an undirected, unweighted graph \mathbf{G} and pattern-enabled system parameters. The continuous dispersion relation crosses the instability threshold (where $\text{Re}(\lambda_\alpha) = 0$) at two points, Λ_{c_1} and Λ_{c_2} , with $\Lambda_{c_1} < \Lambda_{c_2}$. The Laplacian spectrum of \mathbf{G} is ordered²⁸ $\Lambda_0 < \Lambda_1 < \dots < \Lambda_{N-1} = 0$. Suppose further the Laplacian spectrum lies entirely in the stable region and pattern formation does not occur. In other words, $-\Lambda_\alpha < \Lambda_{c_1}$ or $-\Lambda_\alpha > \Lambda_{c_2}$ for all $\alpha = 0, 1, \dots, N-1$.

If we imagine the continuous dispersion relation as a string, and the discrete eigenvalue dispersions as beads on that string, we seek to select just one bead and slide it along the string into the unstable region, while 1) recovering an undirected, unweighted graph from the altered Laplacian spectrum and 2) keeping the other beads (eigenvalues) as close to their original value as possible. This setup is shown in Figure 1

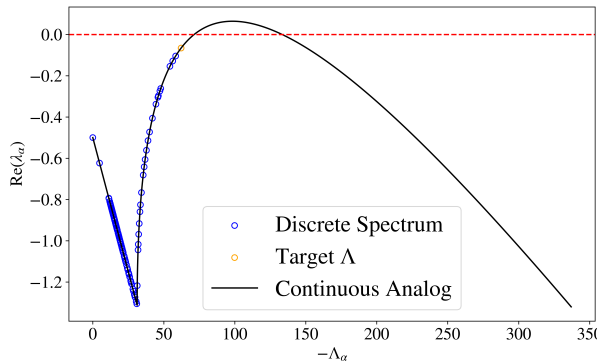


Figure 1: **Initial Setup** A sample continuous and discrete dispersion relation, using a Brusselator model ($\alpha = 2, \beta = 4$) with diffusion coefficients $(D_u, D_v) = (0.01, 0.042)$ and a BA graph on 100 nodes with $m = 15$.

A. Weight-Collapse

We use the prior stabilization procedure as a starting point. When seeking to destabilize just one mode, we alter the first

step of the procedure slightly.

1. (New) After identifying a target mode τ , choose a δ_τ such that $\Lambda_\tau + \delta_\tau$ lies in the instability region, while $\delta_i = 0$ otherwise.

Subsequent steps to generate L_c remain the same. With only one non-zero δ -shift, we achieve a simpler form for $\eta(i, j)$, which we now index by τ .

$$(L_c)_{ij} = L_{ij} + \eta^{(\tau)}(i, j)$$

$$\eta^{(\tau)}(i, j) = (\phi^{(\tau)})_i (\phi^{(\tau)})_j (\delta_\tau)$$

We desire a Laplacian L_f such that $(L_f)_{ij} = \{0, 1\}$ for $i \neq j$, and $(L_f)_{ii} = \sum_{j \neq i} (L_f)_{ij}$. To achieve this, we propose a simple step function, $\mathcal{W} : \mathbb{R} \rightarrow \mathbb{R}$, that collapses values of $\eta^{(\tau)}(i, j)$ depending on a threshold parameter $\theta \in (0, 1)$.

$$\mathcal{W}(x) = \begin{cases} 1 & \text{if } x \leq -\theta \\ 0 & \text{if } x > -\theta \end{cases}$$

After applying this function to off-diagonal entries of L_c , we re-define diagonal entries by calculating row sums of the altered matrix, adding steps (5) and (6) to the control mechanism procedure to form our new matrix L_f , whose eigenvalues are denoted $\Lambda_\alpha^{(f)}$.

5. Form off-diagonal entries of L_f , where $(L_f)_{ij} = \mathcal{W}((L_c)_{ij})$
6. Form diagonal entries of L_f , where $(L_f)_{ii} = -\sum_{j \neq i} (L_f)_{ij}$

Steps (5) and (6) successfully form L_f such that its underlying graph is undirected and unweighted. The transformation $L \rightarrow L_f$ can thus be conceptualized as adding, deleting, or re-wiring edges of L if intermediate re-weightings (captured by L_c) cross a certain threshold θ . Though we have the desired form for L_f , given the intractable nature of analytically deriving the eigenvalues of L_f , there is no clear guarantee that we achieve the desired Laplacian spectrum. We thus turn towards numerical simulations to empirically evaluate the success of this weight-collapse approach.

B. Numerical Simulations

Our simulation recipe involves four ingredients: a graph, system parameters, procedural variables, and evaluation criteria.

1. Graph Choice

We are interested in connected graphs with unweighted, undirected edges. Initial simulations were conducted on Erdős-Rényi (ER), Watts-Strogatz (WS), and Barabási-Albert (BA) graphs, as well as ring lattices. The ring lattice can be seen as a special case of a WS graph in which the re-wiring

probability is 0. Its highly regular structure makes it especially suitable for comparing theoretical predictions with empirical outcomes when studying how edge manipulations induce or suppress instability.

Beyond static graphs, the pattern-formation problem in networks has seen rapid expansion in recent years. Instabilities have been explored on time-varying (temporal) networks^{29,30}, directed networks^{31–33}, Cartesian and higher-dimensional product networks³⁴, and systems with delayed diffusion or reaction dynamics with connections to random walks^{35,36}. These extensions have demonstrated that network structure alone can enable or inhibit pattern formation^{37,38}, even outside classical activator–inhibitor settings. Notably, ring-like structures have been shown to help relax³⁹ the high-diffusion-rate requirements typical of activator–inhibitor models, further motivating their use in analytical studies. Reflecting this broader context clarifies that ring lattices are not an artificial restriction but part of a widely studied class of topologies where structural effects are especially transparent.

Given this landscape, we give special attention to the ring lattice and include additional simulations on it, as its symmetry enables direct comparison between theoretical expectations and empirical results.

2. System Parameters

A number of popular models are used to define the local (reaction) dynamics of species, including but not limited to the Mimura–Murray, Ginzburg–Landau, FitzHugh–Nagumo, and Brusselator models^{40–43}. Without loss of generality, we use the Brusselator model defined below on parameters $\alpha = 2$ and $\beta = 4$:

$$\begin{aligned} f(u_i, v_i) &= \alpha - (\beta + 1)u_i + u_i^2v_i \\ g(u_i, v_i) &= \beta u_i - u_i^2v_i \\ (u^*, v^*) &= (\alpha, \frac{\beta}{\alpha}) \end{aligned}$$

We initialize (D_u, D_v) such that $\text{Re}(\lambda_{\alpha})_{\max} = 0$ for an arbitrary starting value of D_u (here we start with $D_u = 0.01$). Defining $\sigma = \frac{D_v}{D_u}$, our goal in doing this is to initialize $\sigma = \sigma_c$, the critical ratio of diffusion coefficients. We calculate $\sigma > \sigma_c$ such that $\Lambda_{c_2} - \Lambda_{c_1} = |\Lambda_0|$. This creates a Laplacian eigenvalue instability region with width equal to the spectral radius of L . We then choose D_u such that $\Lambda_{c_1} > -\Lambda_\alpha$ for all α , recalculating $D_v = \sigma D_u$. More precisely, we choose D_u such that $\Lambda_{c_1} = -\Lambda_0 + 1$, so the leading eigenvalue is just shy of the Turing instability threshold, with instability region from $-\Lambda_0 + 1$ to $-2\Lambda_0 + 1$. Combined with our choice of α and β , which yield $g_v < 0 < f_u$, we now have a pattern-enabled system.

3. Procedural Variables

We start by setting the weight-collapse threshold $\theta = 0.5$. We choose δ -shifts such that $-(\Lambda_\tau + \delta_\tau) = \frac{1}{2}(\Lambda_{c_1} + \Lambda_{c_2})$,

placing the now unstable target mode in the middle of the instability region before conducting the transformation $L_c \rightarrow L_f$.

4. Evaluation Criteria

To evaluate the success of the proposed control mechanism, we consider both a binary criterion (whether *only* the target mode has been destabilized) and two empirical measures (how far non-target eigenvalues deviate from their initial values and how many edge-changes are needed to go from L to L_f). We define the first empirical measure as the average percentage change of non-target eigenvalues, denoted by $\langle \rho \rangle$. The second, denoted ϵ , is defined as the number of nonzero elements of $A - A_f$, where A and A_f represent the adjacency matrices recovered from L and L_f respectively. We seek to understand the conditions for which any choice of τ satisfies the binary criterion, as well as those for which our empirical measures are minimized.

III. DISCUSSION

A. Simulation Results

For the binary success criterion, while $L \rightarrow L_f$ does not universally succeed in destabilizing some target mode τ , we do have high degrees of success across the domain of τ for certain graphs (see Table I). In failure cases, we observe that we either fail to destabilize $(-\Lambda_\tau^{(f)} < \Lambda_{c_1})$, or some additional mode s is destabilized such that $\Lambda_{c_1} < -\Lambda_s^{(f)} < -\Lambda_\tau^{(f)} < \Lambda_{c_2}$. While we did not observe the case for which τ remained stable by overshooting the instability region (i.e. $-\Lambda_\tau^{(f)} > \Lambda_{c_2}$), we conjecture that it could be possible, potentially by choosing a set of pattern-enabled system parameters with an arbitrarily narrow instability region as well as a large δ_τ . As a final general observation, the binary criterion was more frequently satisfied for Λ_τ close to the instability threshold, consistent with the intuitive expectation that it is harder to de-stabilize modes further in the stability region.

Comparing results across graph types with equal average degree, we observe the success rate for the binary criterion is highest for WS graphs with low rewiring probability ($p = 0.1, 0.2$). ER graphs stand out as those with high variability for success relative to other graph models. BA graphs are exceptionally resilient against this control mechanism, with an average success rate of just 0.16%. Though a large number of edge-changes do occur across all τ values, our control mechanism hardly alters the original Laplacian spectrum of BA graphs, with a general trend indicating an increase in ρ as τ increases. We note that the zero-eigenvalue is always present in a connected graph, so $\tau = N - 1$ always results in failure. See Appendix A, Figures 5 - 9 for further details and sample results for each graph generation model.

We remember from previous discussion that graphs with eigenvectors that demonstrate a high degree of localization can strongly influence the intermediate weighting as we trans-

This is the author's peer reviewed, accepted manuscript. However, the online version of record will be different from this version once it has been copyedited and typeset.
 PLEASE CITE THIS ARTICLE AS DOI: 10.1063/5.0293731

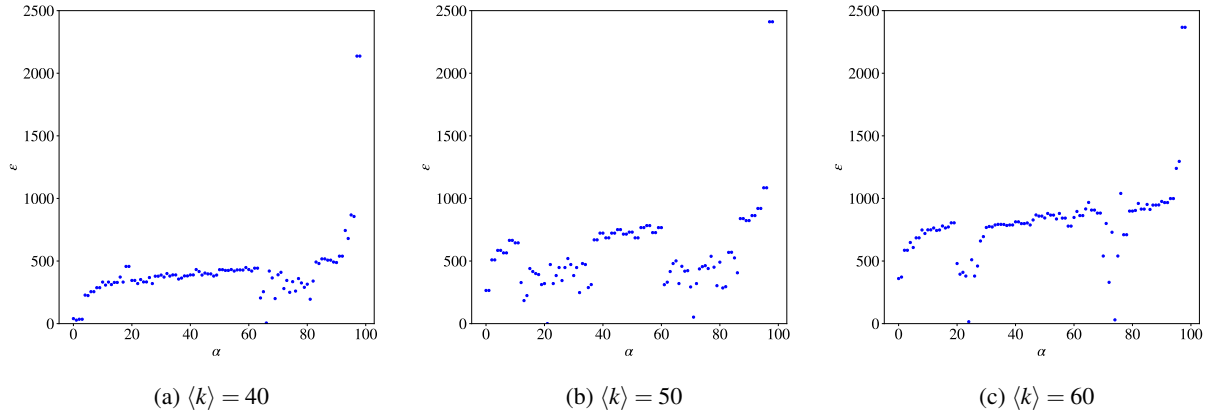


Figure 2: e vs. Target Index Results for ring lattice, $N = 100$

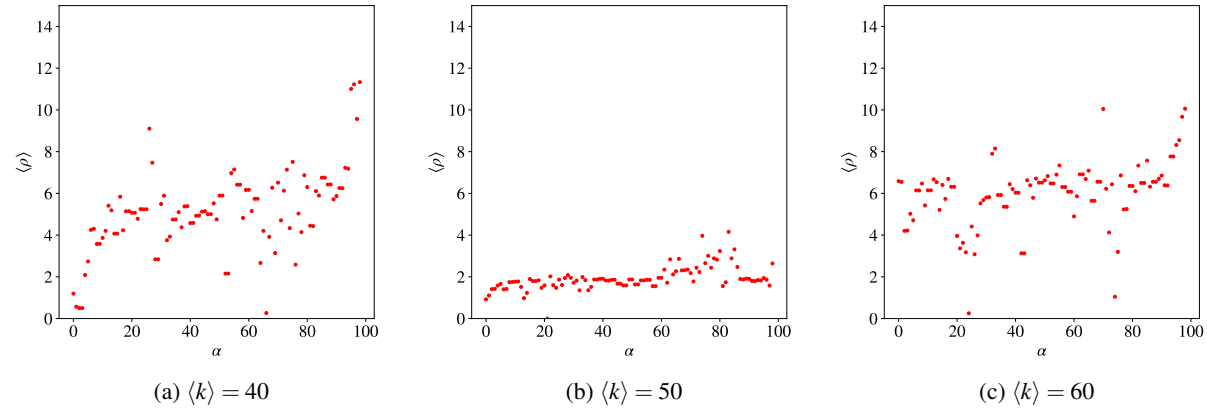


Figure 3: $\langle p \rangle$ vs. Target Index Results for ring lattice, $N = 100$

form from $L \rightarrow L_f$. As shown by Hata and Nakao²⁵ and supplemented by our simulated IPR calculations (see Appendix A), BA graphs display a substantially stronger degree of localization than other tested models. The stark contrast in success and resilience to our control mechanism for BA graphs may be explained in part by this localization, though further experimentation is needed to rigorously evaluate this hypothesis.

We now pay special attention to the case of the ring lattice. Looking at our empirical measures, as shown in Figures 2 and 3, we observe the number of edge changes generally increases as δ_τ increases, but with patches of deviation that depend on $\langle k \rangle$. While the dependence on $\langle k \rangle$ and the nature of deviation patches is unclear, the data otherwise appears to follow the shape of a logit function. The trend for the average percentage change does not demonstrate any statistically significant linear correlations as evaluated by Pearson's correlation coefficient, indicating τ may have less impact on this metric for the ring lattice.

Repeating simulations on variable numbers of nodes, we observe there appears to be a critical number of nodes above which $L \rightarrow L_f$ does not result in any structural changes (i.e. $L_f = L$). Moreover, we found that small θ corresponded to a

higher number of non-edges being converted to edges, while large θ corresponded to higher number of edges being deleted. Though the number of edge changes generally appears to scale with τ , the net change in total degree does not, suggesting the structural changes occurring can largely be conceptualized as re-wiring. Additionally, the edge-changes demonstrate a high degree of symmetry. Sample results are shown in Figure 4, where $\Delta|E|$ denotes the change in edge count between \mathbf{G} and \mathbf{G}_f .

B. Theoretical Bounds for the Ring Lattice

In light of numerical results, we develop theoretical expectations for $L \rightarrow L_f$ when \mathbf{G} is a ring lattice.

Theorem 1. For \mathbf{G} a ring lattice and a target mode τ ,

$$|\eta^{(\tau)}(i,j)| \leq \frac{2}{N} |\delta_\tau|$$

This is the author's peer reviewed, accepted manuscript. However, the online version of record will be different from this version once it has been copyedited and typeset.
 PLEASE CITE THIS ARTICLE AS DOI: 10.1063/5.0293731

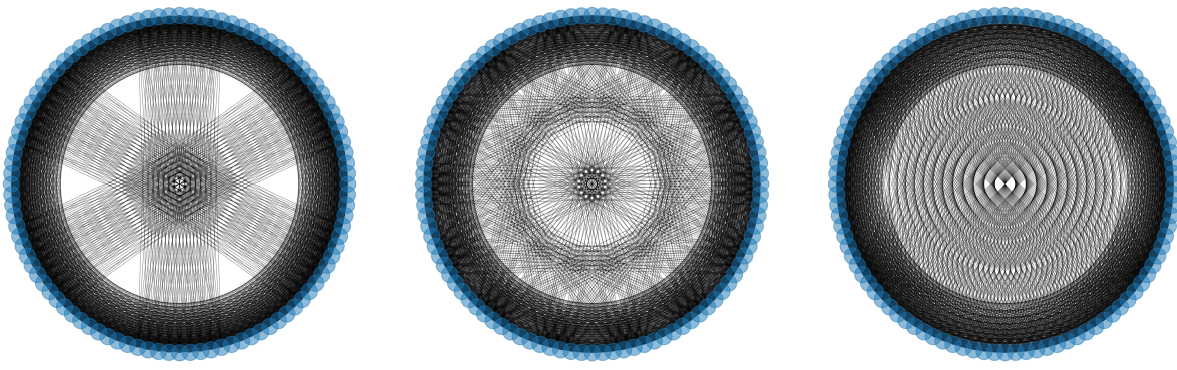


Figure 4: **Symmetric Re-wiring** Visualizations of \mathbf{G}_f for variable τ when \mathbf{G} is a ring lattice and $N = 100$, $\langle k \rangle = 50$

Graph	Mean	Standard Deviation
Ring Lattice	92.93	0
BA	0.16	0.40
ER	82.01	9.08
WS ($p = 0.1$)	97.52	1.68
WS ($p = 0.2$)	93.47	3.07
WS ($p = 0.3$)	91.55	3.23
WS ($p = 0.4$)	91.11	4.76
WS ($p = 0.5$)	91.55	3.69
WS ($p = 0.6$)	90.78	4.75
WS ($p = 0.7$)	89.73	5.18
WS ($p = 0.8$)	90.30	4.95
WS ($p = 0.9$)	90.77	3.64

Table I: **Binary Success Results** Percentage of target eigenvalues fulfilling the binary criterion for various generation models for $N = 100$, $\langle k \rangle = 50$. Expressed as a mean and standard deviation over 100 simulations, where each simulation represents a randomly generated graph tested across all targets.

Proof.

$$L_{ring} = \begin{pmatrix} c_0 & c_1 & c_2 & \dots & \dots & c_{n-1} \\ c_{n-1} & c_0 & c_1 & c_2 & \dots & c_{n-2} \\ \vdots & c_{n-1} & c_0 & c_1 & \ddots & \vdots \\ & & \ddots & \ddots & \ddots & \vdots \\ & & & & & c_1 \\ c_1 & \dots & \dots & \ddots & c_{n-1} & c_0 \end{pmatrix}$$

Observe that the Laplacian for a ring lattice is a circulant matrix. We therefore know its spectrum and eigenvectors in terms of the first row of L_{ring} . Equivalently, the spectrum can be seen as a discrete Fourier transform (DFT) of the first row.

$$\Lambda_\alpha = \sum_{k=0}^{N-1} c_k e^{\frac{2\pi i \alpha}{N} k}$$

$$\phi_j^{(\alpha)} = \frac{1}{\sqrt{N}} (e^{\frac{2\pi i \alpha}{N} j})$$

From this complex eigenbasis, we can derive a real eigenbasis. Namely, for all α , we seek to generate a new eigenvector $\omega^{(\alpha)} \in \mathbb{R}^N$ from $\phi^{(\alpha)} \in \mathbb{C}^N$. Observe that for some complex eigenvector v , at least one of the following statements is true:

1. $v + \bar{v} = 2\text{Re}(v)$ is an eigenvector
2. $i(v - \bar{v}) = -2\text{Im}(v)$ is an eigenvector

Statements (1) and (2) are respectively false when $\text{Re}(v)$ and $\text{Im}(v)$ are the 0 vector. When both are false, v must be the 0 vector, which leads to a contradiction, as the 0 vector is not an eigenvector. Therefore, at least one of (1) and (2) is true.

In our case, $\text{Re}(\phi_j^{(\alpha)}) = \frac{1}{\sqrt{N}} [\cos(\frac{2\pi\alpha}{N} j)]$ and $\text{Im}(\phi_j^{(\alpha)}) = \frac{1}{\sqrt{N}} [\sin(\frac{2\pi\alpha}{N} j)]$. We first ask what happens if we use statement (1) to form real eigenvectors from the real component of $\phi^{(\alpha)}$. Cosine is an even function, so when $\alpha + \beta = N$, $\omega^{(\alpha)} = \omega^{(\beta)}$. Statement (1) therefore only helps us generate a set of $\frac{N}{2} + 1$ unique real eigenvectors for even N and $\frac{N+1}{2}$ for odd N . Statement (2), on the other hand, avoids this symmetry issue, but produces the 0 vector for $\alpha = 0$, and, for even N , $\alpha = \frac{N}{2}$. For these cases⁴⁴ we can leverage statement (1) to produce unique nonzero eigenvectors. After normalizing, we achieve the final set

$$\omega_j^{(\alpha)} = \begin{cases} \frac{-2}{\sqrt{2N}} \sin\left(\frac{2\pi\alpha}{N} j\right) & \text{if } \alpha \notin \{0, \frac{N}{2}\} \\ \frac{1}{\sqrt{N}} \cos\left(\frac{2\pi\alpha}{N} j\right) & \text{if } \alpha \in \{0, \frac{N}{2}\} \end{cases} \quad \text{for } \alpha = 0, 1, \dots, N-1$$

We can now plug into $\eta^{(\tau)}(i, j)$ and consider its maximum.

Case 1: $\tau \notin \{0, \frac{N}{2}\}$

$$\begin{aligned} \max |\eta^{(\tau)}(i, j)| &= \max \left| \frac{2}{N} \sin\left(\frac{2\pi\tau}{N} i\right) \sin\left(\frac{2\pi\tau}{N} j\right) \right| |\delta_\tau| \\ &= \max \left| \frac{1}{N} [\cos\left(\frac{2\pi\tau}{N} (i-j)\right) - \cos\left(\frac{2\pi\tau}{N} (i+j)\right)] \right| |\delta_\tau| \\ &\leq \boxed{\frac{2}{N} |\delta_\tau|} \end{aligned}$$

Case 2: $\tau \in \{0, \frac{N}{2}\}$

$$\begin{aligned} \max |\eta^{(\tau)}(i, j)| &= \max \left| \frac{1}{N} \cos\left(\frac{2\pi\tau}{N}i\right) \cos\left(\frac{2\pi\tau}{N}j\right) |\delta_\tau| \right| \\ &= \max \left| \frac{1}{2N} [\cos\left(\frac{2\pi\tau}{N}(i-j)\right) + \cos\left(\frac{2\pi\tau}{N}(i+j)\right)] \right| |\delta_\tau| \\ &\leq \boxed{\frac{1}{N} |\delta_\tau|} \end{aligned}$$

We have thus proved an upper bound: $|\eta^{(\tau)}(i, j)| \leq \frac{1}{N} |\delta_\tau|$. \square

Theorem 1 is consistent with empirical results as well. Having identified an upper bound on $|\eta^{(\tau)}(i, j)|$, we can further contextualize scenarios in which $L_f = L$. For a chosen τ , let $\tilde{\eta}(\tau)$ denote the actual maximum achieved by $|\eta^{(\tau)}(i, j)|$ over all (i, j) pairs (as opposed to just an upper bound). If

$$\begin{aligned} \tilde{\eta}(\tau) < \theta &\implies (L_f)_{ij} = L_{ij}, \forall L_{ij} = 0 \\ \tilde{\eta}(\tau) < 1 - \theta &\implies (L_f)_{ij} = L_{ij}, \forall L_{ij} = -1 \end{aligned}$$

We have identified separate conditions for which all non-edges remain non-edges and all edges remain edges. When both conditions are satisfied, the weight-collapse function essentially restores L_c to L , resulting in $L_f = L$. This logic similarly supports results indicating that decreasing θ lowered the threshold for edge addition, while increasing θ lowered the threshold for edge deletion.

Corollary 1. For \mathbf{G} a ring lattice, if $\lim_{N \rightarrow \infty} \frac{|\delta_\tau|}{N} = 0$, then there exists some critical number of nodes, N_c , above which $L \rightarrow L_f$ results in $L = L_f$ for a given target and constant $\langle k \rangle$.

The conditional statement is necessary because our choice of N impacts the upper bound of $\tilde{\eta}(\tau)$ in two ways. We see directly an upper bound dependence on N^{-1} , but there is an additional dependence of $|\delta_\tau|$ on N . Our problem set-up requires us to choose δ -shifts that push eigenvalues into the instability region, which we calculate using the gap between the lower threshold (as determined by Λ_0) and Λ_τ . Since the spectrum of L depends on N (and $\langle k \rangle$), and δ_τ depends on the spectrum, δ_τ depends on N . If N grows faster than $|\delta_\tau|$ for increasing N , the maximum possible value of $\tilde{\eta}(\tau)$ (identified in Theorem 1) is driven smaller and smaller, until eventually $\tilde{\eta}(\tau) < \theta$ and $\tilde{\eta}(\tau) < 1 - \theta$ are both necessarily true; no edge-changes occur in this transformation. More precisely, we define

$$N_c = \inf\{N : \tilde{\eta}(\tau) < \min\{\theta, 1 - \theta\}\}$$

Proposition 1. For \mathbf{G} a ring lattice, $\lim_{N \rightarrow \infty} \frac{|\delta_\tau|}{N} = 0$ is always true for constant $\langle k \rangle$.

Proof. We prove Proposition 1 by directly considering $\lim_{N \rightarrow \infty} \frac{|\delta_\tau|}{N}$. We note that the maximum δ -shift will always be δ_F given our problem set-up, where δ_F corresponds to the Fiedler eigenvalue Λ_F . Since shifts are ordered, to prove the limit for all τ , it is sufficient to prove $\lim_{N \rightarrow \infty} \frac{|\delta_\tau|}{N} = 0$

holds for δ_F . We now consider an upper bound on $|\delta_F|$ in terms of N and $\langle k \rangle$. Our scheme dictates δ_τ such that $-(\Lambda_\tau + \delta_\tau) = \frac{1}{2}(\Lambda_{c1} + \Lambda_{c2})$, which we can re-write in terms of the leading eigenvector: $-(\Lambda_\tau + \delta_\tau) = \frac{1}{2}(-3\Lambda_0 + 2)$. Therefore

$$|\delta_F| = \frac{3}{2} |\Lambda_0| - |\Lambda_F| + 1$$

We can put an upper bound on $|\delta_F|$ by using a bound from above for $|\Lambda_0|$ and a bound from below for $|\Lambda_F|$. Namely, via the Perron-Frobenius theorem, $|\Lambda_0| \leq k_{max} = \langle k \rangle$. From⁴⁵, we have $4(N\mathcal{D})^{-1} \leq |\Lambda_F|$, where \mathcal{D} is the diameter of the network. For the ring lattice, we minimize the lower bound on $|\Lambda_F|$ with a maximum possible \mathcal{D} of $\frac{N}{2}$, implying $8N^{-2} \leq |\Lambda_F|$. We now have an upper bound on $|\delta_F|$.

$$|\delta_F| \leq \frac{3}{2} \langle k \rangle - 8N^{-2} + 1$$

It will be sufficient to assume the equality case for maximal $|\delta_F|$, which we plug into our limit of interest.

$$\lim_{N \rightarrow \infty} \frac{|\delta_F|}{N} = \lim_{N \rightarrow \infty} \left(\frac{3\langle k \rangle}{2N} - \frac{8}{N^3} + \frac{1}{N} \right)$$

For constant $\langle k \rangle$, this limit evaluates to 0. We have thus proved $\lim_{N \rightarrow \infty} \frac{|\delta_F|}{N} = 0$, which is sufficient to prove $\lim_{N \rightarrow \infty} \frac{|\delta_\tau|}{N} = 0$. \square

Because $\lim_{N \rightarrow \infty} \frac{|\delta_\tau|}{N} = 0$ is true for the ring lattice, we can assume the existence of N_c . This theoretical result is consistent with the critical number of nodes observed in the numerical simulations, above which $L_f = L$.

Corollary 2. N must be even for $\tilde{\eta}(\tau) = \frac{1}{N} |\delta_\tau|$

The frequency with which $|\eta^{(\tau)}(i, j)|$ reaches its maximum value $\tilde{\eta}(\tau)$ over all (i, j) pairs depends on N, τ . When $\tilde{\eta}(\tau)$ is $\frac{1}{N} |\delta_\tau|$, we require $\tau \notin \{0, \frac{N}{2}\}$ and one of two possible scenarios:

$$\text{Case 1: } \cos\left(\frac{2\pi\tau}{N}(i-j)\right) - \cos\left(\frac{2\pi\tau}{N}(i+j)\right) = 2$$

The argument of the first cosine term must be an integer multiple of 2π , while the argument of the second is an integer multiple of 2π shifted by π .

$$\begin{aligned} \frac{2\pi\tau}{N}(i-j) &= 2\pi\kappa_1 \\ \frac{2\pi\tau}{N}(i+j) &= \pi + 2\pi\kappa_2 \\ \kappa_1, \kappa_2 &\in \mathbb{Z}_+ \end{aligned}$$

We therefore have $\tau(i-j) = N\kappa_1$ and $\tau(i+j) = \frac{N}{2} + N\kappa_2$.

$$\text{Case 2: } \cos\left(\frac{2\pi\tau}{N}(i-j)\right) - \cos\left(\frac{2\pi\tau}{N}(i+j)\right) = -2$$

The argument of the second cosine term must be an integer multiple of 2π , while the argument of the first is an integer multiple of 2π shifted by π .

$$\begin{aligned} \frac{2\pi\tau}{N}(i-j) &= \pi + 2\pi\kappa_1 \\ \frac{2\pi\tau}{N}(i+j) &= 2\pi\kappa_2 \\ \kappa_1, \kappa_2 &\in \mathbb{Z}_+ \end{aligned}$$

We therefore have $\tau(i-j) = \frac{N}{2} + N\kappa_1$ and $\tau(i+j) = N\kappa_2$.

As τ, i, j are all integers, $\tau(i \pm j)$ is an integer as well, so we need $\frac{N}{2}$ to be an integer. Both cases therefore require even N for $\tilde{\eta}(\tau)$ to reach its upper bound.

Proposition 2. *Assume there exists some set of N , denoted \mathbf{N}^* , for which $\tau \in \{0, \frac{N}{2}\}$ guarantees $L = L_f$, while $\tau \notin \{0, \frac{N}{2}\}$ does not. For the special case of $\theta = 1 - \theta = 0.5$, $\mathbf{N}^* = \emptyset$ iff $|\Lambda_F| \leq \frac{|\Lambda_0|}{2} - 1$.*

As a final note, we propose results following from the differing upper bounds of $|\eta^{(\tau)}(i, j)|$ for $\tau \in \{0, \frac{N}{2}\}$ and $\tau \notin \{0, \frac{N}{2}\}$. We prove Proposition 2 by first assuming \mathbf{N}^* is nonempty and attempt to construct its elements.

Here we define \mathbf{N}^* :

$$\begin{aligned} \mathbf{N}_\tau &= \{N : 2|\delta_\tau| < N < 4|\delta_\tau|\} \\ \mathbf{N}^* &= \bigcap_{\tau} \mathbf{N}_\tau \end{aligned}$$

\mathbf{N}_τ is directly obtained by requiring 1) $\frac{1}{N}|\delta_\tau| < \frac{1}{2}$ and 2) $\frac{2}{N}|\delta_\tau| > \frac{1}{2}$. Condition 1) restricts N to the set of values that guarantees $\max |\eta^{(\tau)}(i, j)| < \min\{\theta, 1 - \theta\}$ for $\tau \in \{0, \frac{N}{2}\}$. Condition 2) imposes the restriction that each element of \mathbf{N}^* is less than N_c ; otherwise, we would allow values of N for which $L = L_f$ for all τ . We therefore define a set indexed by τ which includes values of N for which 1) and 2) hold for a given τ , then define \mathbf{N}^* as the intersection of these sets. Because our δ shifts are ordered, we can bypass this two-step process by directly considering the maximum and minimum possible values of $2|\delta_\tau|$ and $4|\delta_\tau|$ respectively.

$$\mathbf{N}^* = \{N : 2 \max_{\tau} |\delta_\tau| < N < 4 \min_{\tau} |\delta_\tau|\}$$

We can re-write the set condition statement as follows.

$$\begin{aligned} 2 \max_{\tau} |\delta_\tau| &< N < 4 \min_{\tau} |\delta_\tau| \\ 2|\delta_F| &< N < 4|\delta_0| \end{aligned}$$

Plugging in from our procedure, we get

$$3|\Lambda_0| + 2 - 2|\Lambda_F| < N < 2|\Lambda_0| + 4 \quad (4)$$

We now directly compare the least and greatest terms of the inequality above.

$$\begin{aligned} 3|\Lambda_0| + 2 - 2|\Lambda_F| &< 2|\Lambda_0| + 4 \\ |\Lambda_F| &> \frac{|\Lambda_0|}{2} - 1 \end{aligned}$$

When $|\Lambda_F| \leq \frac{|\Lambda_0|}{2} - 1$, it is impossible for some N to exist where Inequality 4 is true. As there is no such N that fits the criteria, $\mathbf{N}^* = \emptyset$. This condition describes the gap between the leading and Fiedler eigenvalues and is generally easy to fulfill on random networks, as breaking it requires a very small number of nodes alongside a low average degree. In our numerical simulations, the condition $|\Lambda_F| \leq \frac{|\Lambda_0|}{2} - 1$ was always fulfilled, and we accordingly observed $\mathbf{N}^* = \emptyset$.

IV. CONCLUSION

In addition to rigorously developing fundamentals of network Turing patterns, our work analyzes a new topological control mechanism for targeted mode destabilization, building a deeper theoretical understanding of structurally mediated Turing patterns for the ring lattice. There are a number of related research questions spawning from these results. For instance, existing topological control studies typically "draw their conclusions by comparing two different static network topologies."⁴⁶ Such is the case in our work, as we treat the control intervention as a discrete shift from one static architecture (L) to another (L_f). Applying this work to temporal networks, whose topologies can change over continuous time, could prove to be a promising research space. Furthermore, given the stark difference in success for networks with varying degrees of Laplacian eigenvector localization, future studies might seek to understand the relationship between degree heterogeneity, localization, and pattern emergence. Though we pay special attention to the ring lattice, there are further unexplored directions for this graph type, such as quantifying pattern invariance when destabilizing different targets. Lastly, attempting to prove boundedness results similar to Theorem 1 on random graphs could prove a fruitful endeavor as well. Ultimately, this work seeks to enhance our theoretical understanding of pattern formation in light of the omnipresent and salient real-world examples of reaction-diffusion systems on networks.

DATA AVAILABILITY STATEMENT

The data that support the findings of this study are available from the corresponding author upon reasonable request.

Appendix A: Supplementary Results from Numerical Simulations

This is the author's peer reviewed, accepted manuscript. However, the online version of record will be different from this version once it has been copyedited and typeset.
 PLEASE CITE THIS ARTICLE AS DOI: 10.1063/5.0293731

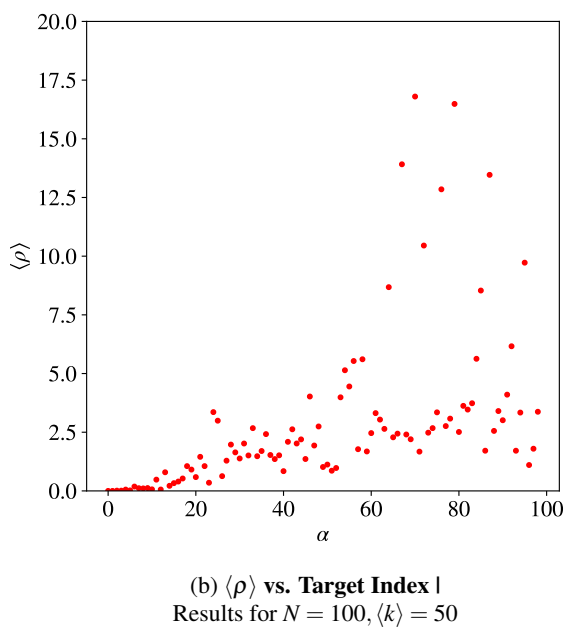
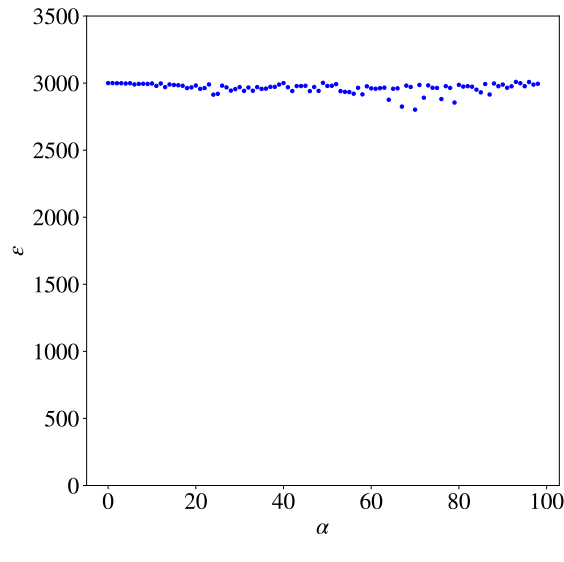


Figure 5: BA Model averaged over 100 runs

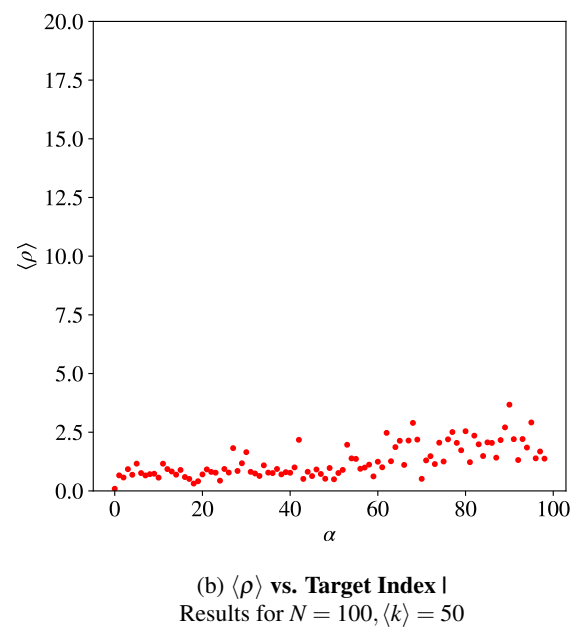
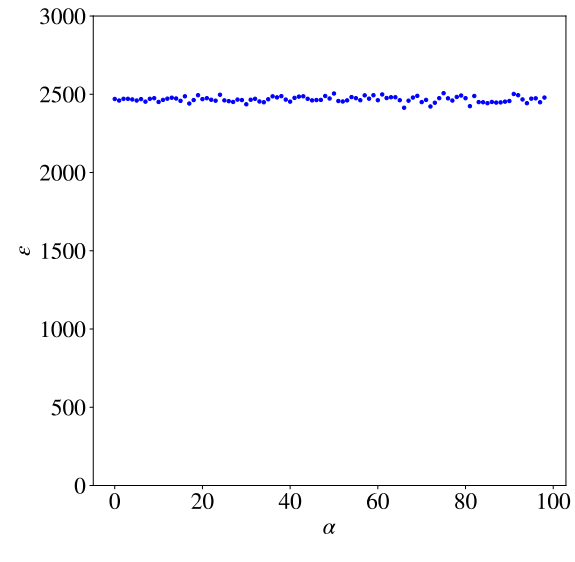


Figure 6: ER Model averaged over 100 runs

This is the author's peer reviewed, accepted manuscript. However, the online version of record will be different from this version once it has been copyedited and typeset.
 PLEASE CITE THIS ARTICLE AS DOI: 10.1063/5.0293731

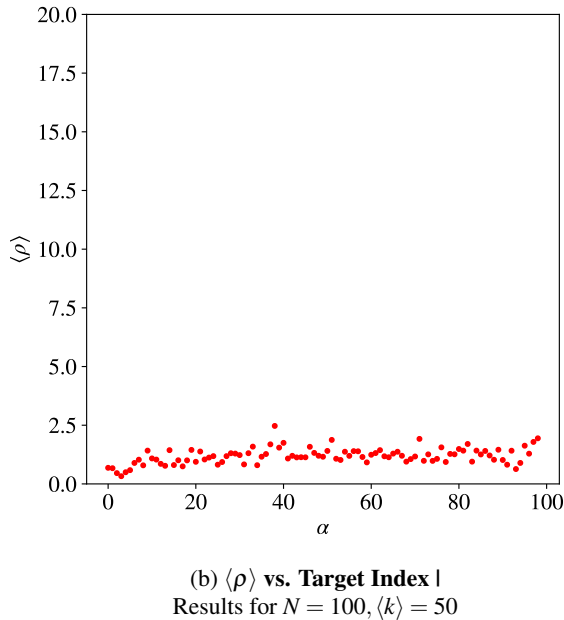
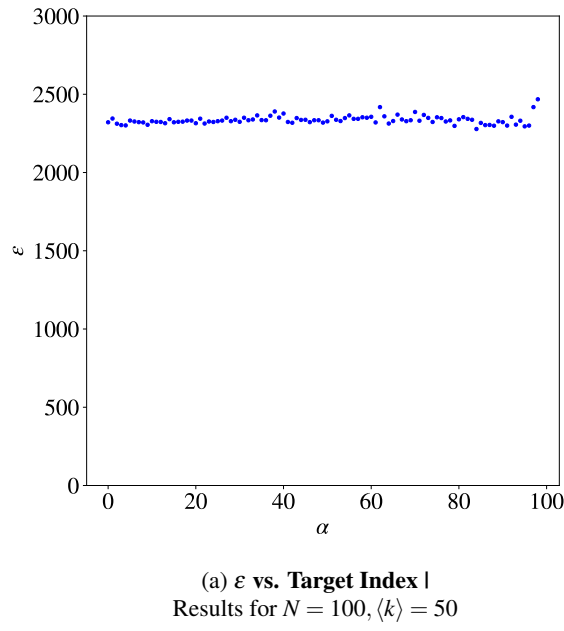


Figure 7: WS Model averaged over 100 runs, $p = 0.1$

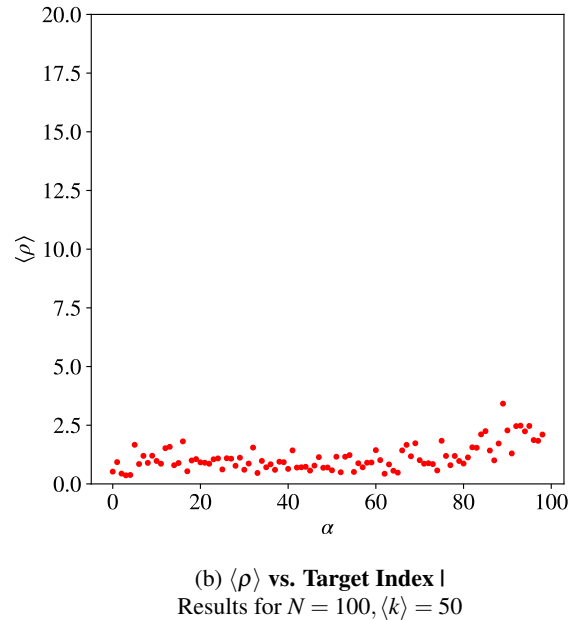
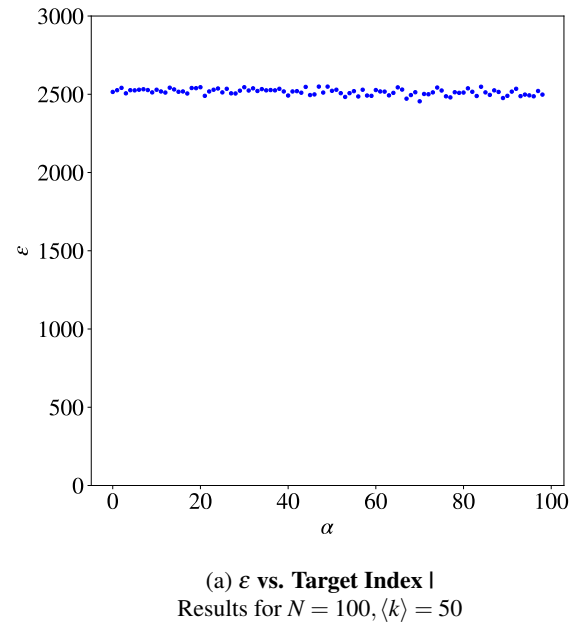


Figure 8: WS Model averaged over 100 runs, $p = 0.5$

This is the author's peer reviewed, accepted manuscript. However, the online version of record will be different from this version once it has been copyedited and typeset.
 PLEASE CITE THIS ARTICLE AS DOI: 10.1063/5.0293731

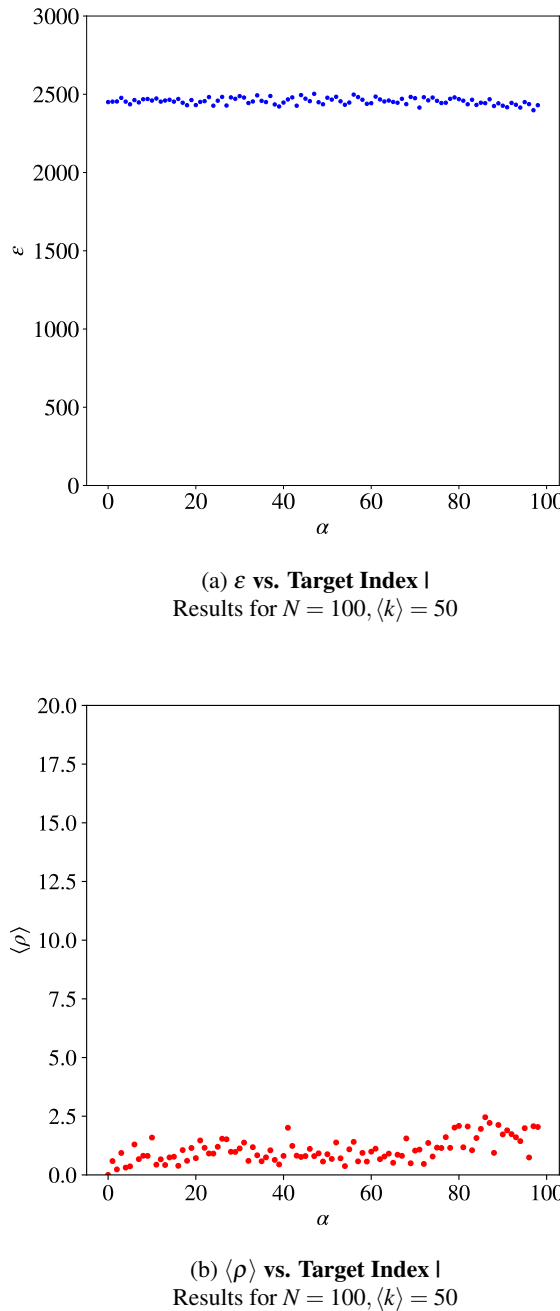


Figure 9: WS Model averaged over 100 runs, $p = 0.9$

Graph	Mean
Ring Lattice	0.054
BA	0.417
ER	0.049
WS ($p = 0.1$)	0.059
WS ($p = 0.5$)	0.041
WS ($p = 0.9$)	0.046

Table II: **IPR Scores** Average localization score across all eigenvectors for various models when $N = 100$, $\langle k \rangle = 50$. Expressed as a mean over 100 simulations.

REFERENCES

- ¹G. Cencetti, F. Bagnoli, G. Battistelli, L. Chisci, F. Di Patti, and D. Fanelli, The European physical journal. B, Condensed matter physics **90**, 1 (2017), place: Berlin/Heidelberg Publisher: Springer Berlin Heidelberg.
- ²A. M. Turing, Bulletin of Mathematical Biology **52**, 153 (1990).
- ³J. H. E. Cartwright, Journal of Theoretical Biology **217**, 97 (2002).
- ⁴A. Mondal, R. K. Upadhyay, A. Mondal, and S. K. Sharma, Applied Mathematics and Computation **423**, 127010 (2022).
- ⁵E. M. Rauch and M. M. Millonas, Journal of Theoretical Biology **226**, 401 (2004).
- ⁶V. Giunta, M. C. Lombardo, and M. Sammartino, SIAM Journal on Applied Dynamical Systems **20**, 1844 (2021).
- ⁷M. M. Zheng, B. Shao, and Q. Ouyang, Journal of Theoretical Biology **408**, 88 (2016).
- ⁸P. Ball, Philosophical Transactions of the Royal Society B: Biological Sciences **370**, 20140218 (2015), publisher: Royal Society.
- ⁹L. Shen and R. Van Gorder, Journal of Theoretical Biology **420** (2017), publisher: Elsevier.
- ¹⁰C. Liu, L. Chang, Y. Huang, and Z. Wang, Nonlinear Dynamics **99**, 3313 (2020).
- ¹¹M. Song, S. Gao, C. Liu, Y. Bai, L. Zhang, B. Xie, and L. Chang, Chaos, solitons and fractals **168**, 113131 (2023), publisher: Elsevier Ltd.
- ¹²N. Zaker, C. A. Cobbold, and F. Lutscher, Mathematical Biosciences and Engineering **19**, 2506 (2022), number: 3 Publisher: AIMS Press.
- ¹³T. Takaguchi and R. Lambiotte, Journal of Theoretical Biology **380**, 134 (2015), arXiv:1410.5116 [cond-mat, physics:physics, q-bio].
- ¹⁴M. Duan, L. Chang, and Z. Jin, Physica A: Statistical Mechanics and its Applications **533**, 122023 (2019).
- ¹⁵W. Wang, X. Gao, Y. Cai, H. Shi, and S. Fu, Journal of the Franklin Institute **355**, 7226 (2018).
- ¹⁶R. Pastor-Satorras and A. Vespignani, Physical Review Letters **86**, 3200 (2001), publisher: American Physical Society.
- ¹⁷This design is an intentional but not mandatory choice following from Fick's law⁴⁷. Additional mechanisms can be designed that account for a given species' diffusion as a function of the concentrations of all species rather than just that of the diffusing species. As an example, such a design might prove apt for predator-prey scenarios in which the movement of a prey species intuitively depends on both surrounding prey and predator populations.
- ¹⁸M. Asllani, T. Carletti, and D. Fanelli, The European physical journal. B, Condensed matter physics **89**, 1 (2016), place: Berlin/Heidelberg Publisher: Springer Berlin Heidelberg.
- ¹⁹G. Cencetti, P. Clusella, and D. Fanelli, Scientific Reports **8**, 16226 (2018), number: 1 Publisher: Nature Publishing Group.
- ²⁰H. Nakao and A. S. Mikhailov, Nature Physics **6**, 544 (2010).
- ²¹Y. Ide, H. Izuohara, and T. Machida, Physica A **457**, 331 (2016), publisher: Elsevier B.V.
- ²²Note that there is no sign guarantee on δ_l , as we can push the eigenvalue to either side of the unstable region of the dispersion relation. The original publication does not specify a convention.
- ²³Since L is real symmetric Laplacian, we can choose an eigenbasis with all real eigenvector entries. We thus write Φ^T rather than the conjugate transpose Φ^\dagger , knowing $\Phi^\dagger = \Phi^T = \Phi^{-1}$ in this case.

This is the author's peer reviewed, accepted manuscript. However, the online version of record will be different from this version once it has been copyedited and typeset.

- ²⁴Though not universally appropriate for modeling real-world phenomena, negative-weights are salient in a number of network science applications, including financial and transportation networks among others.
- ²⁵S. Hata and H. Nakao, *Scientific Reports* **7**, 1121 (2017), number: 1 Publisher: Nature Publishing Group.
- ²⁶S. Mimar, M. M. Juane, J. Park, A. P. Muñozuri, and G. Ghoshal, *Physical review. E* **99**, 062303 (2019), place: United States Publisher: American Physical Society APS.
- ²⁷P. N. McGraw and M. Menzinger, *Physical Review E* **77**, 031102 (2008), arXiv:0708.4206 [cond-mat].
- ²⁸We change index from 0 to $N - 1$ for ease of notation in future circulant matrix calculations.
- ²⁹S. Zhou, Y. Guo, M. Liu, Y.-C. Lai, and W. Lin, *Physical review. E* **100**, 032302 (2019), publisher: American Physical Society.
- ³⁰J. Petri, B. Lauwens, D. Fanelli, and T. Carletti, *Physical Review Letters* **119**, 148301 (2017), publisher: American Physical Society.
- ³¹H. Zhang, Y. Sheng, and Z. Zeng, *IEEE Transactions on Neural Networks and Learning Systems* **29**, 1550 (2018).
- ³²M. Asllani, J. D. Challenger, F. S. Pavone, L. Sacconi, and D. Fanelli, *Nature Communications* **5**, 4517 (2014), number: 1 Publisher: Nature Publishing Group.
- ³³J. Ritchie, *Communications in nonlinear science & numerical simulation* **116**, 106892 (2023), publisher: Elsevier B.V.
- ³⁴M. Asllani, D. M. Busiello, T. Carletti, D. Fanelli, and G. Planchon, *Physical Review E* **90**, 042814 (2014), publisher: American Physical Society.
- ³⁵C. Falco, *Physical Review E* **106**, 054103 (2022), arXiv:2206.08859 [physics].
- ³⁶T. Carletti, M. Asllani, D. Fanelli, and V. Latora, *Physical Review Research* **2**, 033012 (2020).
- ³⁷Q. Xuan, F. Du, H. Dong, L. Yu, and G. Chen, *Physical Review E* **84**, 036101 (2011), publisher: American Physical Society.
- ³⁸X. Diego, L. Marcon, P. Müller, and J. Sharpe, *Physical review. X* **8**, 021071 (2018), place: College Park Publisher: American Physical Society.
- ³⁹M. Asllani, T. Carletti, D. Fanelli, and P. K. Maini, *The European Physical Journal B* **93**, 135 (2020).
- ⁴⁰M. Mimura and J. Murray, *Journal of Theoretical Biology* **75**, 249 (1978).
- ⁴¹Q. Zheng and J. Shen, *Computers & Mathematics with Applications* **70**, 1082 (2015).
- ⁴²B. Peña and C. Pérez-García, *Physical Review E* **64**, 056213 (2001), publisher: American Physical Society.
- ⁴³I. S. Aranson and L. Kramer, *Reviews of Modern Physics* **74**, 99 (2002), publisher: American Physical Society.
- ⁴⁴Noting that $\frac{N}{2}$ is not in the domain of α for odd N , we henceforth collectively treat the 0-vector cases as the cases in which $\alpha \in \{0, \frac{N}{2}\}$ without loss of generality.
- ⁴⁵B. Mohar, E. Y. Alavi, G. Chartrand, O. R. Oellermann, and A. J. Schwenk, *Graph theory, combinatorics, and applications*.
- ⁴⁶R. A. Van Gorder, *Proceedings of the Royal Society A: Mathematical, Physical and Engineering Sciences* **477**, rspa.2020.0753, 20200753 (2021).
- ⁴⁷J. Lowney and R. Larrabee, *IEEE Transactions on Electron Devices* **27**, 1795 (1980), conference Name: IEEE Transactions on Electron Devices.